ACS OMEGA

http://pubs.acs.org/journal/acsodf

Article

Transformation of Waste Toner Powder into Valuable Fe_2O_3 Nanoparticles for the Preparation of Recyclable Co(II)-NH_2-SiO_2@Fe_2O_3 and Its Applications in the Synthesis of Polyhydroquinoline and Quinazoline Derivatives

Mobina Kouser, Bushra Chowhan, Neha Sharma, and Monika Gupta*

Cite This: *ACS Omega* 2022, 7, 47619−47633

Read Online

ACCESS | Metrics & More | Article Recommendations | Supporting Information

ABSTRACT: Ecological recycling of waste materials by converting them into valuable nanomaterials can be considered a great opportunity for management and fortification of the environment. This article deals with the environment-friendly synthesis of Fe_2O_3 nanoparticles (composed of α-Fe_2O_3 and γ-Fe_2O_3) using waste toner powder (WTP) *via* calcination. Fe_2O_3 nanoparticles were then coated with silica using TEOS, functionalized with silane (APTMS), and immobilized with Co(II) to get the desired biocompatible and cost-effective catalyst, *i.e.*, Co(II)-NH_2-SiO_2@Fe_2O_3. The structural features in terms of evaluation of morphology, particle size, presence of functional groups, polycrystallinity, and metal content over the surface were determined by Fourier transform infrared spectroscopy (FTIR), powder X-ray diffraction (P-XRD), field emission gun-scanning electron microscopy (FEG-SEM), energy-dispersive X-ray analysis (EDX), high resolution-transmission electron microscopy (HR-TEM), X-ray photoelectron spectroscopy (XPS), thermogravimetric analysis (TGA), vibrating sample magnetometry (VSM), Brunauer−Emmett−Teller (BET) analysis, and inductively coupled plasma-atomic emission spectroscopy (ICP-AES) studies. XPS confirmed the (II) oxidation state of Co, and ICP-AES and EDX supported the loading of Co(II) over the surface of the support. P-XRD proved the polycrystalline nature of the Fe_2O_3 core and even after functionalization. In comparison to previously reported methods, Co(II)-NH_2-SiO_2@Fe_2O_3 provides an eco-friendly procedure for the synthesis of polyhydroquinoline and quinazoline derivatives with several advantages such as a short reaction time and high yield. Polyhydroquinoline and quinazoline derivatives are important scaffolds in pharmacologically active compounds. Moreover, the developed nanocatalyst was recyclable, and HR-TEM and P-XRD confirmed the agglomeration in the recycled catalyst resulted in a decrease in yield after the fifth run. The present protocol provides a new strategy of recycling e-waste into a heterogeneous nanocatalyst for the synthesis of heterocycles *via* multicomponent reactions. This made the synthesized catalyst convincingly more superior to other previously reported catalysts for organic transformations.

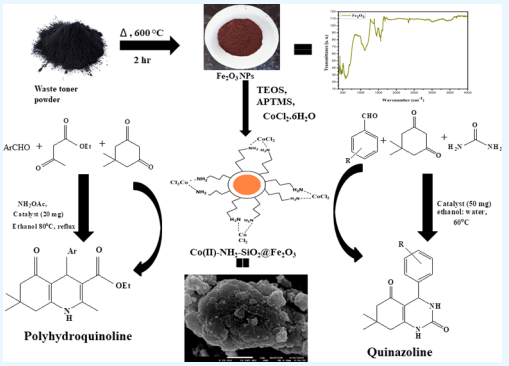

1. INTRODUCTION

Nanocatalysis consolidates the positive aspects of homogeneous and heterogeneous catalysis methods while reducing their drawbacks.[1] Nanocatalysts act as linkers between homogeneous and heterogeneous catalysts,[2] exhibiting nearly 100% selectivity, high activity, and good yield with improved product separation and catalytic recovery. The numerous advantages of heterogeneous catalysts such as effortless workup procedure, recyclability, good dispersion, and high selectivity and activity gave the heterogeneous catalysts a lead over their homogeneous counterparts. Taking into consideration the need for a sustainable environment, we want to use waste materials as support systems for the nanocatalyst. The advancement and utilization of electronic equipment led to the generation of a huge amount of fast-growing electronic waste in the world. Among the electronic waste, discarded waste toner powder (WTP) from printer devices releases ∼6000 tons of processed carbon powder into the atmosphere.[3] Synthesis of nanocatalysts from waste materials as sources is an alternative route leading to sustainability and green chemistry. Waste toner disposed of by traditional methods is hard to degrade, resulting in soil and underground water pollution. Waste toner is a granular mixture and comprises about 7.0 wt % polyacrylate, 55.0 wt % polystyrene, 3.0 wt % SiO_2, and 35.0 wt % Fe_3O_4.[4] Around 62.0 wt % toner waste comprises organic

Received: July 18, 2022
Accepted: November 23, 2022
Published: December 15, 2022

Scheme 1. General Procedure for the Synthesis of Co(II)-NH_2-SiO_2@Fe_2O_3

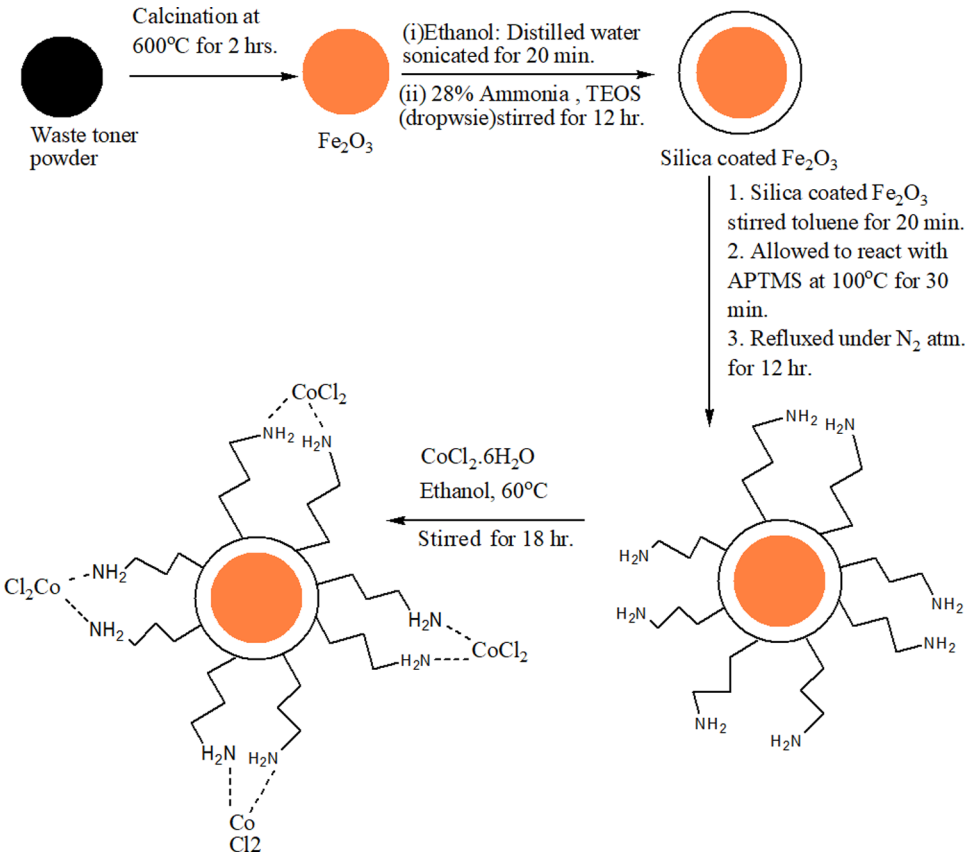

components, which might bring diseases such as cancer to human bodies. At present, many researchers are focusing on recycling waste toner into valuable constructive materials such as synthetic oils,[5] nano-SiO_2, SiO_2-carbon, nano-Fe_3O_4,[6,7] fillers,[8] and colorants[9] in the rubber manufacturing process. Waste toner powder can be successfully transformed and recycled into (3D) graphene oxide (GO),[10] Fe_2O_3/g-C_3N_4,[11] and FeO-NC[12] by thermal transformation techniques to escape handling hazards.

Isolated neat Fe_2O_3 magnetic nanoparticles (MNPs) have relatively low colloidal stability, which lead to aggregation of nanoparticles (NPs), especially at higher concentrations, and have high nonspecific binding.[13] Therefore, modification or coating of iron oxide nanoparticles is important to improve their stability and biocompatibility and prevent leaching of the magnetic core into the reaction medium under harsh conditions.[14] Further, functionalization with various functional groups such as amine groups, phenyl groups, thiol groups, and aliphatic hydrocarbons has been reported.[14−17] Herein, we focus on surface functionalization with 3-aminopropyltrimethoxysilane (APTMS) to introduce NH_2, which is necessary to further facilitate coordination with the metal atom or metal ion.

Cobalt catalysts have attracted substantial attention in organic synthesis owing to their higher reactivity in organic transformations, low cost, nontoxicity, availability, and their interesting mode of action as compared to other transition metals.[18−22] Multicomponent reactions (MCRs) could be employed to obtain complex products from readily available starting materials in an environment-friendly manner. Polyhydroquinoline and quinazoline derivatives are potent fused heterocycles that emerged as versatile bioactive compounds possessing both biological and pharmaceutical activities.[23,24] Polyhydroquinoline derivatives are important five-membered *N*-containing heterocycles. These pharmaceutically active compounds have drawn a lot of attention. They exhibited diverse therapeutic properties such as vasodilator, hepatoprotective, antiatherosclerotic, bronchodilator, antitumor, geroprotective, and antidiabetic activities and showed a tendency to modulate calcium channels.[25,26] Quinazoline derivatives also act as diuretics, vasodilating, tranquilizing, antitumor, antidefibrillatory, antibiotic, antihistaminic, anticonvulsant, anticancer, and herbicidal agents and play a role in plant growth activity.[27−29] Therefore, the synthesis of these heterocycles has gained interest in organic synthesis. However, most of the synthetic routes to the synthesis of polyhydroquinoline and quinazoline derivatives offer many drawbacks such as long reaction, high temperature, low yield, harsh reaction conditions, use of sonication and microwave irradiation, stability, and reusability of the catalyst.[25,30,31] Thus, we synthesized an environmentally benign nanomaterial, *i.e.*, Co(II)-silane-functionalized SiO_2-coated Fe_2O_3 (Co(II)-NH_2-SiO_2@Fe_2O_3), and used it to synthesize polyhydroquinoline and quinazoline derivatives with a significant yield in a low reaction time under mild conditions.

2. EXPERIMENTAL SECTION

2.1. Materials and Chemicals. All of the chemical materials required for the synthesis of the catalyst, polyhydroquinolines, and quinazolines were purchased from Sigma-Aldrich and TCI chemicals with high purity. All of the chemicals were used without further purification.

https://doi.org/10.1021/acsomega.2c04512
ACS Omega 2022, 7, 47619−47633

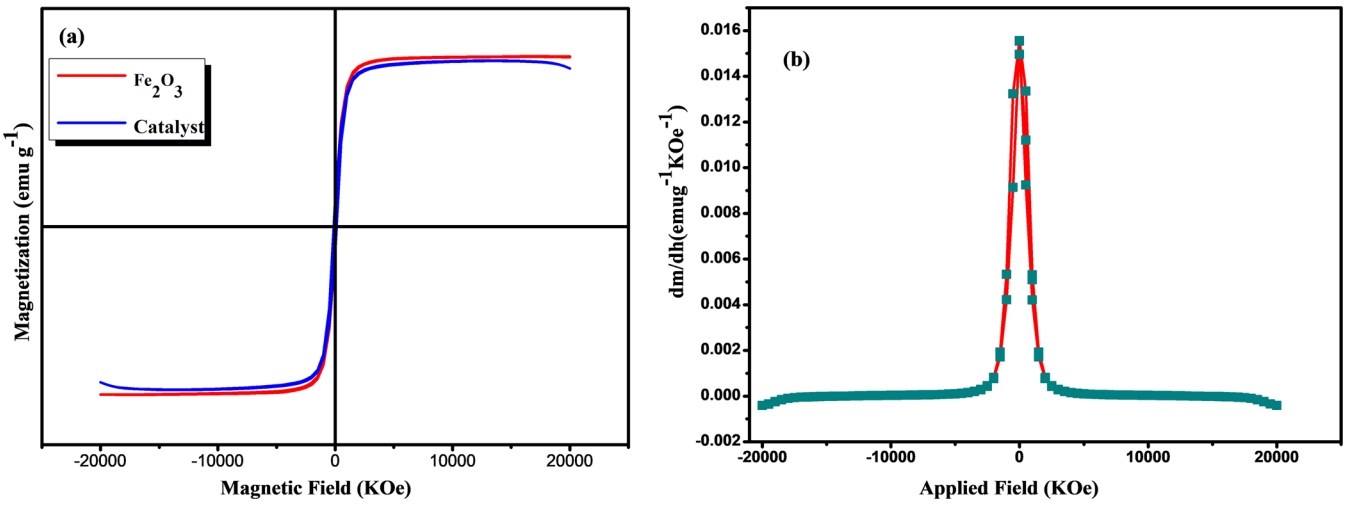

Figure 1. VSM spectra of Co(II)-NH_2-SiO_2@Fe_2O_3 (a). Room-temperature dM/dH versus H curves for Co(II)-NH_2-SiO_2@Fe_2O_3 (b).

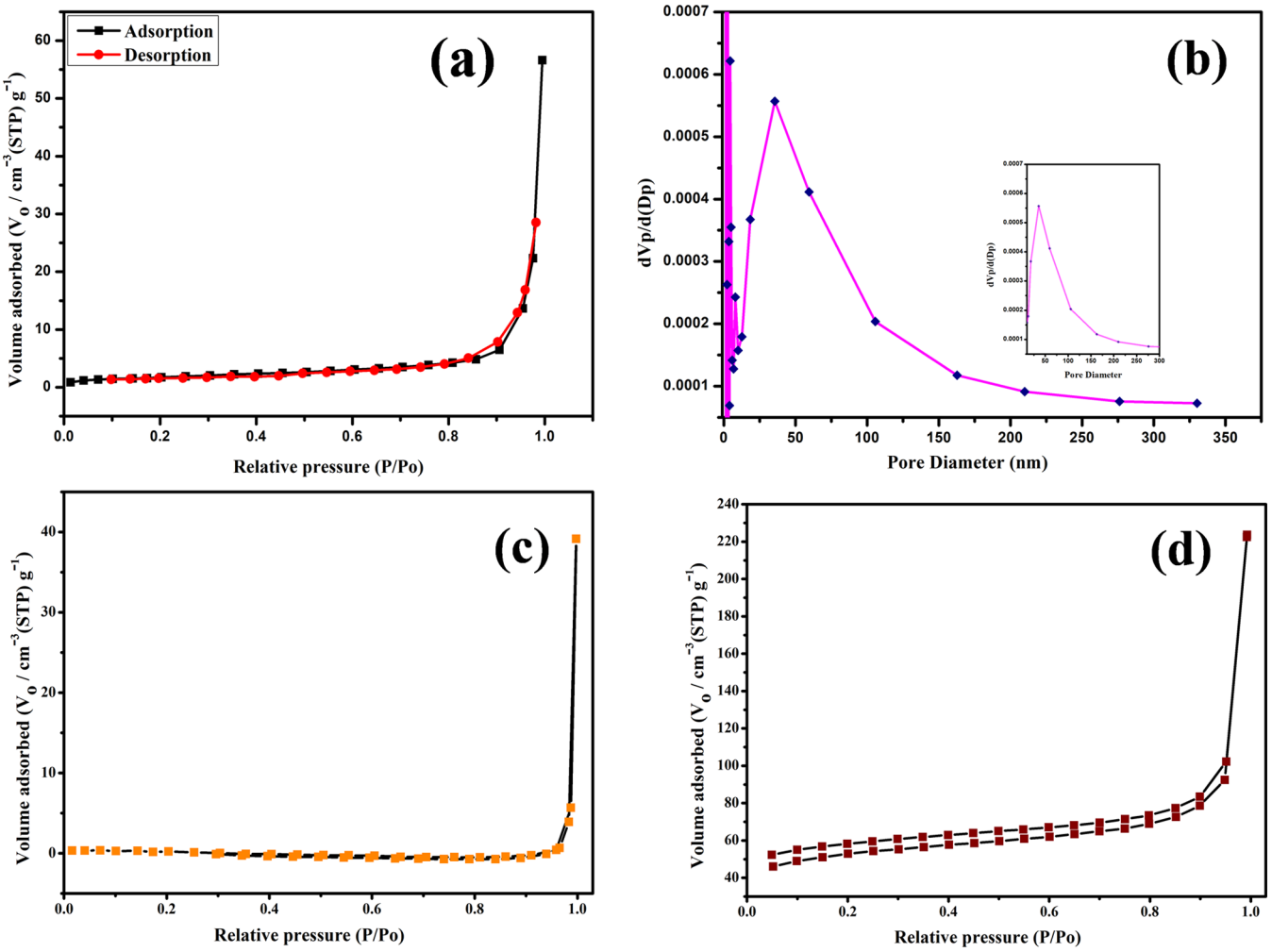

Figure 2. Nitrogen adsorption−desorption isotherm of the Co(II)-NH_2-SiO_2@Fe_2O_3 catalyst (a). BJH pore size distribution curve of Co(II)-NH_2-SiO_2@Fe_2O_3 (b). Nitrogen adsorption−desorption isotherm of NH_2-SiO_2@Fe_2O_3 (c). Nitrogen adsorption−desorption isotherm of Co(II)-SiO_2@Fe_2O_3 (d).

2.2. Preparation of Co(II)-NH_2-SiO_2@Fe_2O_3. *2.2.1. Synthesis of Fe_2O_3 from Waste Toner Powder (WTP).* WTP (5 g) was collected from waste print cartridges, and then, the collected waste toner was calcined at 600 °C for 2 h in a muffle furnace to obtain Fe_2O_3 (2.26 g). The obtained Fe_2O_3 magnetic nanoparticles (MNPSs) dispersed in isopropyl alcohol and were sonicated for about 90 min.

https://doi.org/10.1021/acsomega.2c04512
ACS Omega 2022, 7, 47619−47633

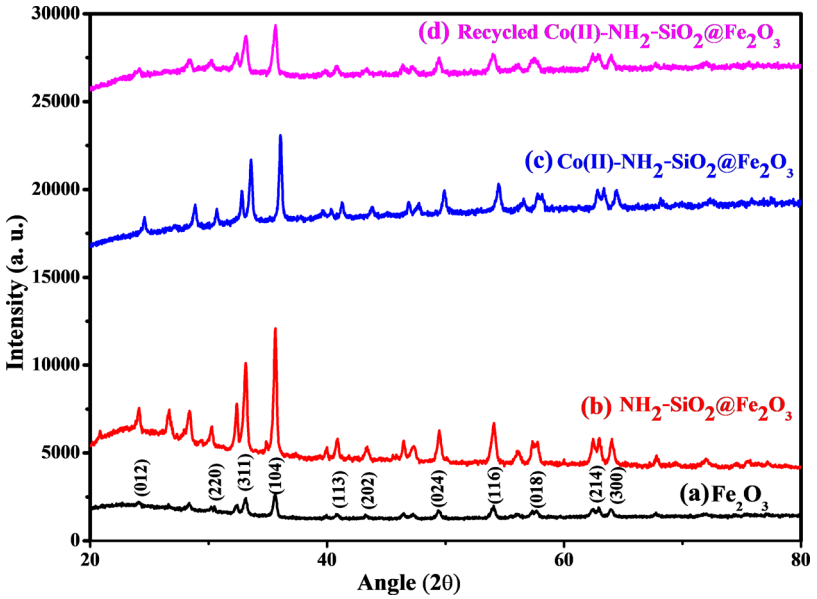

Figure 3. P-XRD spectra of Fe_2O_3 (a), NH_2-SiO_2@Fe_2O_3 (b), Co(II)-NH_2-SiO_2@Fe_2O_3 (c), and recycled Co(II)-NH_2-SiO_2@Fe_2O_3 (d).

2.2.2. Synthesis of Silica-Coated Fe_2O_3 Using TEOS as the Precursor. Fe_2O_3 (2 g) was treated with HNO_3 (0.1 M, 60 mL) followed by ultrasonication for 20 min. The treated Fe_2O_3 were dispersed in a mixture of ethanol and distilled water (20:20) *via* ultrasonication for 20 min. The solution was then transferred to a round-bottomed flask, followed by the dropwise addition of ammonia (28%, 3.4 mL) and tetraethoxysilane TEOS (15 mL) under vigorous stirring at room temperature. After stirring for 12 h, nanoparticles were separated by filtration, washed with ethanol and water, and dried in a desiccator overnight.

2.2.3. Synthesis of Silane-Functionalized SiO_2@Fe_2O_3. After successful coating of silica, SiO_2@Fe_2O_3 (2.315 g) nanoparticles were dispersed in toluene (100 mL) for 20 min by stirring to obtain a homogeneous solution. Then, the dispersed nanoparticles were reacted with 3-aminopropyltrimethoxysilane APTMS (4.65 mL) first at 100 °C for 30 min, and then, the solution was refluxed under a N_2 atmosphere for 12 h. The prepared silane-functionalized SiO_2@Fe_2O_3 was filtered, washed with toluene several times, and dried in an oven at 60 °C for 6 h.

2.2.4. Synthesis of Co(II) Immobilized Silane-Functionalized SiO_2@Fe_2O_3. The synthesized silane-functionalized SiO_2@Fe_2O_3 nanoparticles were stirred in an ethanolic solution of $CoCl_2$ (1.5 g in 20 mL of ethanol) for 18 h at 60 °C. The final catalyst was then filtered, washed with ethanol 3 times, and dried in a desiccator overnight.

2.3. Catalytic Application in the Synthesis of Heterocycles. *2.3.1. General Procedure for the Synthesis of Polyhydroquinoline Derivatives.* To a round-bottomed flask, a mixture of aldehyde (1 mmol), dimedone (1 mmol), ethylacetoacetate (1 mmol), and ammonium acetate (1.2 mmol) was added in, followed by the addition of Co(II)-NH_2-SiO_2@Fe_2O_3 (20 mg) and ethanol (3 mL). The mixture was stirred at 80 °C under a reflux for an appropriate time, and the reaction was monitored by TLC. After the reaction was completed, hot ethanol was added to dissolve the product and to separate the catalyst. The filtrate was evaporated to obtain the solid product. It was crystallized using ethanol to get the pure product.

2.3.2. General Procedure for the Synthesis of Quinazoline Derivatives. To a mixture of aldehyde (1 mmol), dimedone (1 mmol), and urea (1 mmol) in an ethanol/H_2O (1:1) mixture, Co(II)-NH_2-SiO_2@Fe_2O_3 (50 mg) was added. The reaction mixture was heated at 60 °C, and progress of the reaction was continuously monitored using TLC. After the completion of the reaction, the mixture was dissolved in dichloromethane, and the catalyst was separated by filtration. The product was obtained after evaporation of the solvent, and crystallization was done using ethanol.

3. RESULTS AND DISCUSSION

3.1. Catalyst Synthesis and Characterization. Preparation of Co(II) immobilized on silane-functionalized silica-coated Fe_2O_3 MNPs consisted of four major steps, as shown in Scheme 1. (i) Calcination of waste toner into polycrystalline Fe_2O_3 at 600 °C for 2 h. (ii) Coating of Fe_2O_3 with SiO_2 using TEOS as a precursor by the sol–gel method. Ethanol–water mixture was chosen as the solvent to obtain a homogeneous reaction mixture. SiO_2 as a surface modifier was chosen to transfer Fe_2O_3 magnetic nanoparticles from the organic phase to the aqueous phase, which imparted excellent biocompatibility and facile conjugation with various functional groups to the whole system. (iii) Surface functionalization of silica MNPs with APTMS, which effectively improved the mechanical properties of silica coating. (iv) Immobilization of $CoCl_2$ on the NH_2-functionalized silica-coated MNPs for catalytic activity. The catalytic activity of the prepared heterogeneous nanocatalyst was well characterized and studied by various techniques.

The magnetic properties of the prepared nanocatalyst were studied by a vibrating sample magnetometer (VSM). The

Table 1. Crystallographic Data Obtained from XRD of Fe_2O_3.

	lattice parameters (Å)			
sample	*a*	*b*	*c*	crystallite size (nm)
Fe_2O_3	5.0351	5.0351	13.7483	32.07

https://doi.org/10.1021/acsomega.2c04512
ACS Omega 2022, 7, 47619−47633

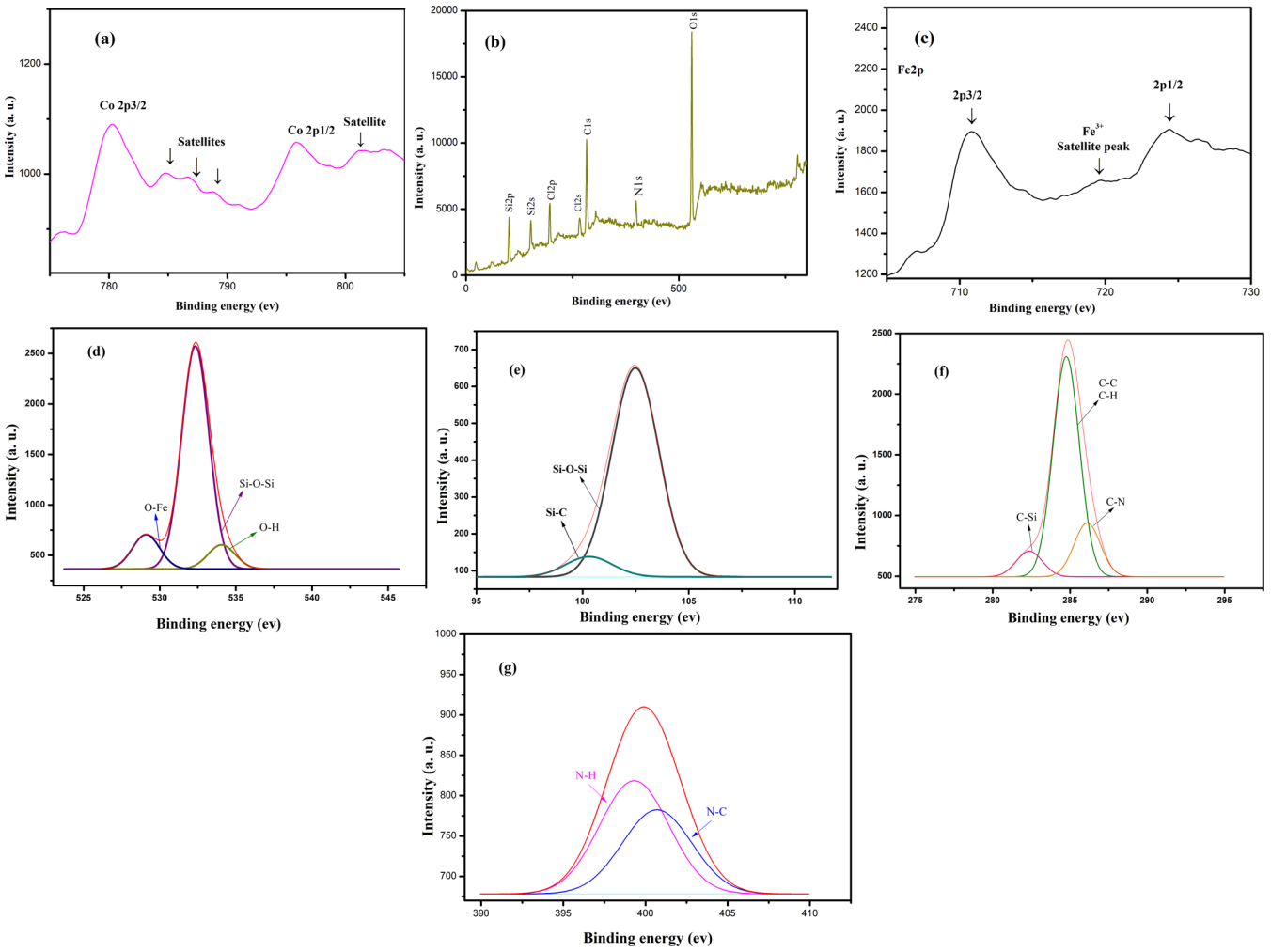

Figure 4. XPS spectra of Co(II)-NH_2-SiO_2@Fe_2O_3 (a) Co(II) 2p region, (b) Su region, (c) Fe 2p region, (d) O 1s, (e) Si 2p, (f) C 1s, and (g) N 2p.

curve showed that the catalyst exhibited a small magnetic hysteresis and a soft ferromagnetic state, as illustrated in Figure 1a. The saturated magnetization values (Ms) of Fe_2O_3 and the catalyst, *i.e.*, Co(II)-NH_2-SiO_2@Fe_2O_3, were found to be 19.5 and 14.25 emu g^{-1}, respectively. On comparison with Fe_2O_3, the magnetization value decreased, which can be attributed to the presence of nonmagnetic silane-functionalized silica coating on the surface of Fe_2O_3 MNPs during the synthetic route of the nanocatalyst.[32] The single peak near zero of the magnetic field in the dM/dH versus H curve (Figure 1b) further confirmed the soft magnetic nature of the synthesized Co(II)-NH_2-SiO_2@Fe_2O_3 nanocatalyst. Moreover, it also proved the single magnetic domain-type nature of the developed nanocatalyst.[33]

N_2 adsorption−desorption isotherm spectrum was conducted to calculate the porous properties and surface area of the developed nanocatalyst. The BET isotherms of Co(II)-NH_2-SiO_2@Fe_2O_3 and Co(II)-SiO_2@Fe_2O_3 were studied, as shown in Figure 2a,d. The presence of the H4 hysteresis loop along with the type IV isotherm, which was the characteristic feature of mesoporous materials, was noticed. Co(II)-NH_2-SiO_2@Fe_2O_3 possesses the BET surface area of 16.39 m^2 g^{-1} with the total pore volume and mean diameter pore as 0.00626 cm^3 g^{-1} and 29.47 nm, respectively, whereas Co(II)-SiO_2@Fe_2O_3 has surface area 12 m^2 g^{-1}. Based on this data, Co(II)-NH_2-SiO_2@Fe_2O_3 produced a larger surface area than Co(II)-SiO_2@Fe_2O_3 with improved surface exposure of the active catalytic sites and had better catalytic activity in organic transformations. Figure 2b exhibits the BJH pore size distribution curve of Co(II)-NH_2-SiO_2@Fe_2O_3. It indicates that most of the pores in the developed nanocatalyst fall in the range of 30−48 nm. To study the effect of Co(II) loading on silane-functionalized silica-coated Fe_2O_3, BET analysis of NH_2-SiO_2@Fe_2O_3 was also carried out as shown in Figure 2c. Based on the analysis, the BET surface area and pore size volume were 10 m^2 g^{-1} and 0.3128 cm^3 g^{-1}, respectively.

Powder X-ray diffraction (P-XRD) spectra showed the crystallinity of the developed nanocatalyst. Figure 3a reveals that when waste toner powder was annealed at 600 °C two major XRD peaks at 33.19 and 35.63° were registered for the α and γ phases of Fe_2O_3, respectively, which correspond to the (104) and (311) crystalline planes (JCPDS no. 39-1346).[34,35] The other less intense peaks at 24.1, 30.21, 40.8, 43.25, 49.44, 54.00, 57.50, 62.95, and 63.95° matched with (012), (220), (113), (202), (024), (116), (018), (214), and (300) planes of the α phase of Fe_2O_3, respectively (JCPDS card no. 33-0664).[36] Lattice parameters of the synthesized Fe_2O_3 nanoparticles are tabulated in Table 1. As presented in Figure 3a, the peak position and their relative intensities indicated that there was no preferred orientation, which suggested the

https://doi.org/10.1021/acsomega.2c04512
ACS Omega 2022, 7, 47619−47633

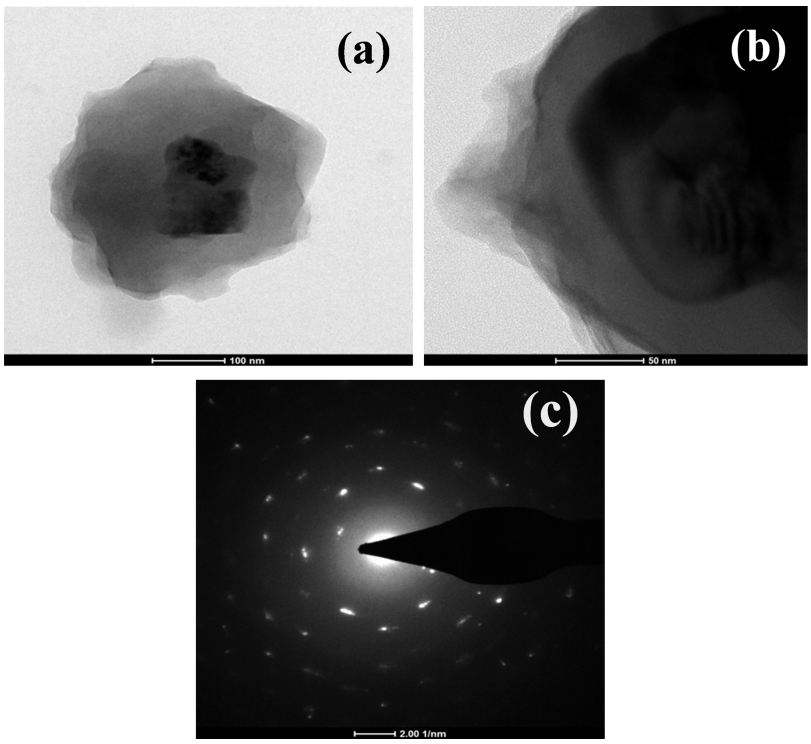

Figure 5. HR-TEM micrographs of Co(II)-NH_2-SiO_2@Fe_2O_3 (a, b). SAED pattern of Co(II)-NH_2-SiO_2@Fe_2O_3 (c).

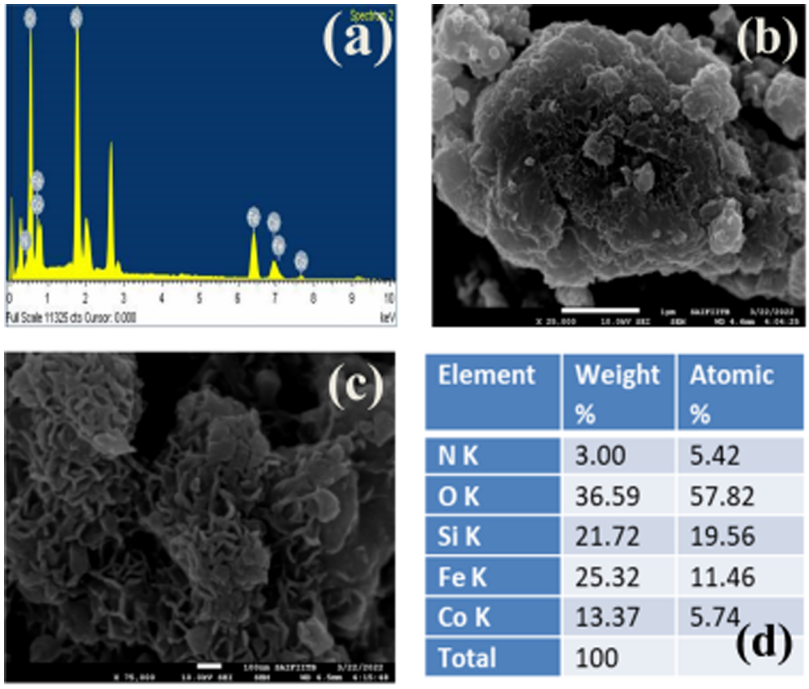

Figure 6. EDX spectra of Co(II)-NH_2-SiO_2@Fe_2O_3 (a). FEG-SEM images of Co(II)-NH_2-SiO_2@Fe_2O_3 (b, c). EDX analysis of Co(II)-NH_2-SiO_2@Fe_2O_3 (d).

formation of polycrystalline Fe_2O_3 (composed of γ-Fe_2O_3 and α-Fe_2O_3), which was in good agreement with the SAED pattern (Figure 5c).[37] Therefore, for the complete decomposition of organic residues present in the toner powder and the phase transformation of Fe_3O_4 into Fe_2O_3, calcination of the toner powder was carried out at 600 °C for 2 h. The average crystallite sizes of Fe_2O_3 and Co(II)-NH_2-SiO_2@Fe_2O_3 were estimated to be 32.07 and 42.44 nm, respectively, calculated using Scherrer's formula[38] based on the measurements of FMHW of their most intense peaks. Figure 3c represents the P-XRD of Co(II)-NH_2-SiO_2@Fe_2O_3; on comparing it with the P-XRD pattern of Fe_2O_3, it was observed that there was a significant enhancement in the peak intensity, which contributed toward more crystallinity of Fe_2O_3 on further heating. Further, on comparing it with Figure 3b, there was an extra hump at 2θ from 20 to 28°, which reflected

https://doi.org/10.1021/acsomega.2c04512
ACS Omega 2022, 7, 47619−47633

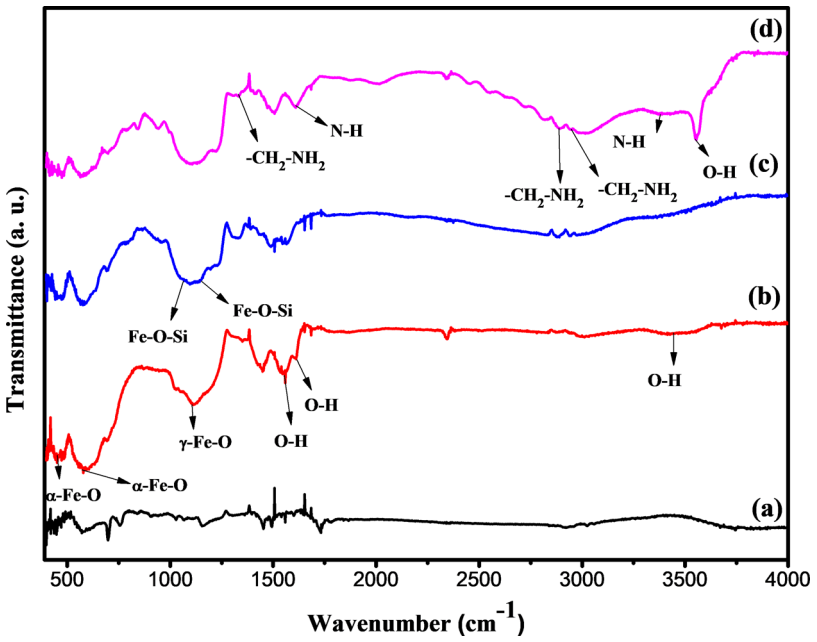

Figure 7. FTIR spectra of waste toner powder (WTP) (a), Fe_2O_3 (b), Fe_2O_3@SiO_2 (c), and Co(II)-NH_2-SiO_2@Fe_2O_3 catalyst (d).

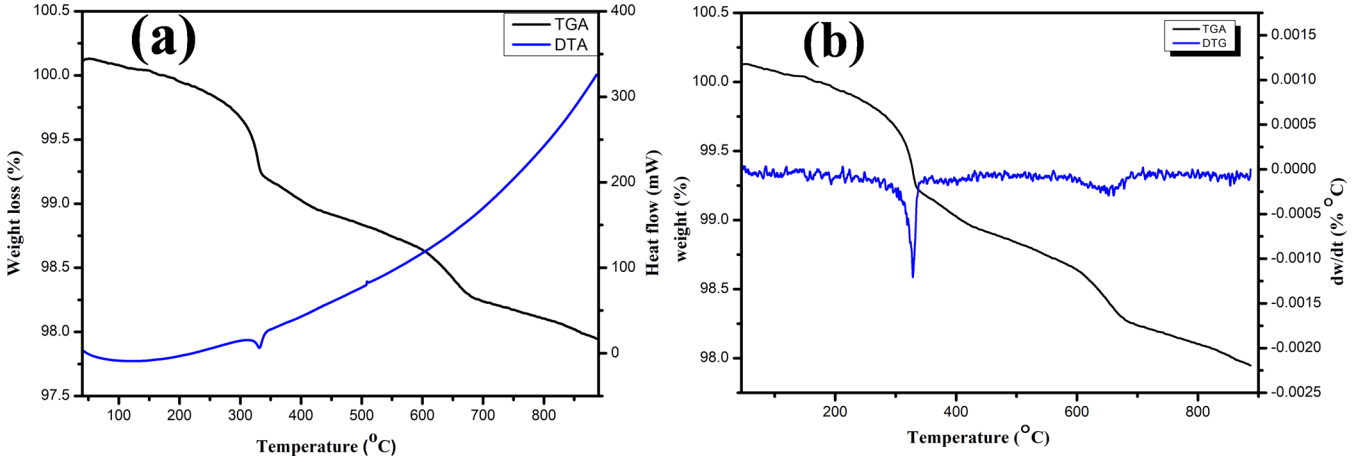

Figure 8. Thermogravimetric analysis (TGA) and differential thermal analysis (DTA) of Co(II)-NH_2-SiO_2@Fe_2O_3 (a). Thermogravimetric analysis (TGA) and differential thermogravimetric (DTG) plot of Co(II)-NH_2-SiO_2@Fe_2O_3 (b).

the presence of silica. Owing to the low content of Co(II) compared to Fe_2O_3 and its tetrahedral coordination with two NH_2 endings of silane on the surface, characteristic peaks of Co(II) were not observed in the XRD pattern (Figure 3c).[39] Further, on reusability, the catalyst showed a decrease in intensities of P-XRD peaks after the fifth run, which was probably due to deformations and agglomeration of the catalytic structure (Figure 3d).

The elemental composition and oxidation state of cobalt in the catalyst were inspected by XPS. The two binding energy peaks at 780.24 and 795.92 eV, which can be assigned to Co $2p_{3/2}$ and Co $2p_{1/2}$ electronic states of Co(II) state, are shown in Figure 4a.[40] The presence of satellites in the XPS spectra is the characteristic of paramagnetic compounds.[41] The energy splitting (ΔE) between Co $2p_{3/2}$ and Co $2p_{1/2}$ was found to be 15.7 eV, consistent with Co(II).[42] In the overview XPS spectra (Figure 4b), peaks of the iron element were not observed and peaks of silica, nitrogen, oxygen, chlorine, and carbon were observed. This confirmed the Fe_2O_3 core was completely enclosed with a silica shell and functionalized with APTMS.[32] From Figure 4c, the spectra of Fe exhibited an Fe $2p_{3/2}$ peak at 710.8 eV, an Fe $2p_{1/2}$ peak at 724.4 eV, and a satellite peak at 719.5 eV. These are the characteristics peaks of Fe^{3+} confirming the conversion of waste toner into Fe_2O_3. Binding energy peaks at 534.1, 532.4, and 529 eV confirmed the O−H, Si−O−Si, and O−Fe bonds, respectively, shown in Figure 4d.[43,44] The peaks at 102.3 and 100.2 eV in Figure 4e confirmed the presence of Si−O−Si and Si−C bonds, respectively.[45] The C 1s spectra showed four different contributions as shown in Figure 4f; the binding energy peaks at 285, 282.2, 286, and 285 eV were related to C−C, C−Si, C−N, and C−H bonds, respectively.[43] In addition, the N 1s spectra (Figure 4g) showed the presence of N−C and N−H bonds at peaks 400.7 and 399.3 eV, respectively.[46,47]

HR-TEM images were studied to investigate the morphology of the nanocatalyst. In these images, the spherical geometry of Fe_2O_3 magnetic nanoparticles, which further embraced numerous small clusters of crystal grains ranging

https://doi.org/10.1021/acsomega.2c04512
ACS Omega 2022, 7, 47619−47633

Table 2. One-Pot Synthesis of Polyhydroquinoline Derivatives with Different Aldehydes *via* the Hantzsch Reaction Catalyzed by Co(II)-NH_2-SiO_2@Fe_2O_3[a,b]

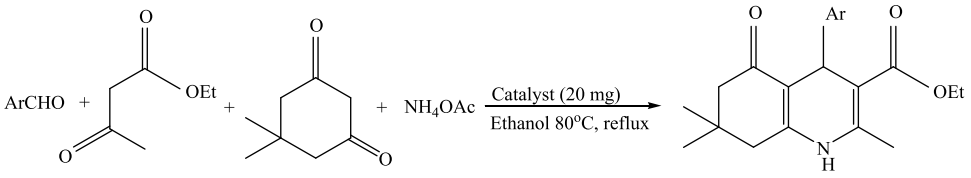

S.No.	Aldehyde	Time (min.)	Yield (%)[b]	Product
1	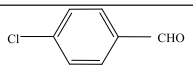	14	95	2a
2	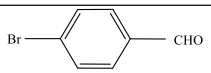	14	95	2b
3	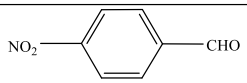	14	95	2c
4	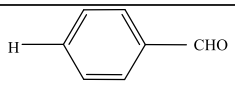	13	95	2d
5	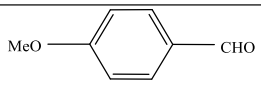	15	94	2e
6	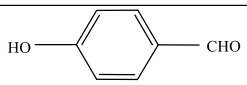	15	94	2f
7	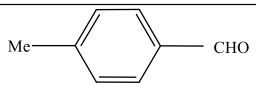	14	95	2g
8	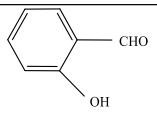	16	94	2h
9	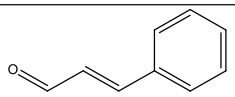	21	92	2i
10	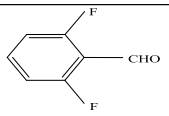	13	95	2j
11	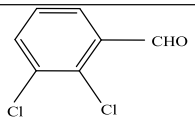	14	95	2k
12	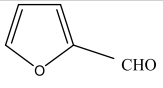	17	92	2l
13	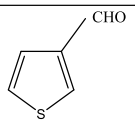	19	91	2m

[a]Optimized reaction conditions: aldehyde (1 mmol), dimedone (1 mmol), ethylacetoacetate (1 mmol), and ammonium acetate (1.2 mmol) in ethanol. [b]Isolated yields.

https://doi.org/10.1021/acsomega.2c04512
ACS Omega 2022, 7, 47619−47633

Table 3. Effect of Temperature and Catalyst in the One-Pot Synthesis of Polyhydroquinoline[a]

entry	catalyst (mg)	temp. (°C)	time (min)	yield (%)[b]
1		100	60	41
2	Fe_2O_3	100	60	41
3	Fe_2O_3@SiO_2-Co(II)	100	60	80
5	Co(II)-NH_2-SiO_2@Fe_2O_3 (50)	100	15	95
6	Co(II)-NH_2-SiO_2@Fe_2O_3 (30)	60	15	91
7	Co(II)-NH_2-SiO_2@Fe_2O_3 (20)	40	15	90
8	Co(II)-NH_2-SiO_2@Fe_2O_3 (50)	r.t.	60	85
9	**Co(II)-NH_2-SiO_2@Fe_2O_3 (20)**	**80**	**15**	**95**

[a]Optimized reaction conditions: Aldehyde (1 mmol), dimedone (1 mmol), ethylacetoacetate (1 mmol) and ammonium acetate (1.2 mmol) in ethanol. [b]Isolated yields.

Table 4. Effect of Solvent in the One-Pot synthesis of Polyhydroquinoline[a]

entry	solvent	time (min)	yield (%)[b]
1	no solvent	45	89
2	water	35	92
3	ethanol:water	17	92
4	CH_3CN	60	56
5	**ethanol**	**15**	**95**
6	DCM	90	41

[a]Optimized reaction conditions: 4-chlorobenzaldehyde (1 mmol), dimedone (1 mmol), ethylacetoacetate (1 mmol), and ammonium acetate (1.2 mmol) in ethanol. [b]Isolated yields.

from nanometer to the micrometer range, was observed. The existence of silica coating and silane around the Fe_2O_3 nanoparticles was confirmed by TEM images (Figure 5a,b). In addition, a clear boundary was seen between the Fe_2O_3 nanoparticle core and the silica shell. Figure 5c shows the polycrystalline nature of the developed nanocatalyst, which was in good agreement with the interpretation of P-XRD. The morphology of the catalyst was also examined by FEG-SEM analysis (Figure 6b,c). The spectra demonstrated the layered structure of the catalyst, *i.e.*, wrinkled silica coating and silane functionalization over the surface of iron oxide. Further, the EDX spectrum showed the elemental composition of the catalyst, where the presence of Fe, O, Si, N, C, and Co(II) is evident (Figure 6a,c). The ICP-AES analysis indicated that the Co(II) content loaded onto 50 mg of Co(II)-NH_2-SiO_2@Fe_2O_3 was found to be 6.95 wt %.

The formation and functional groups present in the catalyst were further analyzed by Fourier transform infrared FTIR spectroscopy. Figure 7 shows the FTIR spectra of waste toner powder (WTP) (a), Fe_2O_3 (derived from waste toner powder) (b), Fe_2O_3@SiO_2 (c), and Co(II)-NH_2-SiO_2@Fe_2O_3 (d). In the spectrum of waste toner powder, in Figure 7a, a broad peak was observed after 3100 cm^{-1}, which was attributed to black carbon vibrations. The band in the region from 400 to 1200 cm^{-1} presented vibrations of different iron oxides. However, other peaks were assigned to the polymer additives.[48] The FTIR spectra of Fe_2O_3 showed peaks at about 464 and 583 cm^{-1} due to the stretching and bending vibrations of the Fe−O bond of γ-Fe_2O_3, while an intense peak at 1112 cm^{-1} exhibited the vibration of the Fe−O bond of α-Fe_2O_3.[32,38,43] There was also a broad peak at 3450, 1609, and 1560 cm^{-1}, attributed to the stretching and bending vibrations of hydrogen bonded O−H on the surface of Fe_2O_3.[43,49−51] The intense broad IR absorption peak shown in Figure 7c from 1084 to 1131 cm^{-1} was due to the vibration of the Fe−O−Si bond and the Si−O−Si bond, respectively (refs 43, 52, 53). Figure 7d displays peaks at 2947, 2895, and 1332 cm^{-1}, indicating the stretching vibration of $-CH_2-NH_2$ and the wagging and twisting vibrations of $-CH_2-NH_2$, respectively, of the APTMS fragment. In addition, there was a broad hump from 3300 to 3442 cm^{-1} and a peak at 1609 cm^{-1} assigned to the stretching and scissoring vibrations of N−H in NH_2. These peaks were of very low intensity, confirming the successful tetrahedral coordination of Co(II) to two NH_2 endings.[54] At 1609 cm^{-1}, the peak of O−H stretching on the Fe_2O_3 surface reduced and prominent N−H bending peak appeared, as shown in Figure 7d. These results demonstrated the successful coating, functionalization around Fe_2O_3, and coordination of Co(II) on the surface (Figure 8).

Thermogravimetric analysis (TGA) was used to determine the thermal stability of the nanocatalyst where loss in mass of the catalyst by heating up to 900 °C was presented. The initial weight loss of 0.895% observed on heating at 328 °C was probably due to the evaporation of adsorbed solvents from the atmosphere and entrapped water molecules. The second weight loss of 1.84% observed in the range from 350 to 685 °C was due to decomposition of the silica shell from the nanoparticle surface and the cracking of the siloxane chain Si−O−Si.[53] The differential thermogravimetric (DTG) plot displayed two endothermic peaks, while just one endothermic peak was observed in the differential thermal analysis (DTA) of Co(II)-NH_2-SiO_2@Fe_2O_3.

3.1.1. Catalytic Testing for the One-Pot Synthesis of Polyhydroquinoline Derivatives. The catalytic activity of the prepared nanocatalyst was explored in the synthesis of polyhydroquinoline and quinazoline derivatives. The various effective factors for the reaction such as the amount of catalyst, solvent, and temperature were studied to determine optimal reaction conditions for the one-pot synthesis of polyhydroquinoline derivatives. Initially, *p*-chlorobenzaldehyde (1 mmol), dimedone (1 mmol), ethylacetoacetate (1 mmol), and ammonium acetate (1 mmol) were chosen as model substrates for the reaction (Table 2, entry 1).

As shown in Tables 2−4, aldehyde (1 mmol), dimedone (1 mmol), ethylacetoacetate (1 mmol), and ammonium acetate (1.2 mmol) in the presence of 20 mg of catalyst in ethanol at 80 °C under reflux conditions were found to be ideal reaction conditions for the one-pot synthesis of polyhydroquinoline derivatives. It is worth mentioning that only 40% of the desired product was isolated in the absence of the catalyst after 60 min at 100 °C (Table 3, entry 1). Table 2 clearly indicates the scope of the reaction with respect to aliphatic, aromatic, and heterocyclic aldehydes. The results verified that both electron-donating and electron-withdrawing aromatic aldehydes worked well, leading to good yield of products. However, the time taken for the completion of the reaction was longer with aromatic aldehyde substituted with electron-donating groups as compared to electron-withdrawing groups. Among the heterocyclic aldehydes, indole-3-carboxaldehyde gave the best result, but yields were very moderate as compared to aromatic aldehydes (Table 2, entry 12).

A plausible mechanism for the polyhydroquinoline synthesis is shown in Scheme 2.[55] According to the literature, the formation of a product goes by two different paths. In this mechanism, Co(II)-NH_2-SiO_2@Fe_2O_3 acts as a Brønsted acid that contributes to the Knoevenageal condensation of

https://doi.org/10.1021/acsomega.2c04512
ACS Omega 2022, 7, 47619−47633

Scheme 2. Possible Mechanistic Pathway for the Synthesis of Polyhydroquinoline in the Presence of the Co(II)-NH_2-SiO_2@ Fe_2O_3 Catalyst

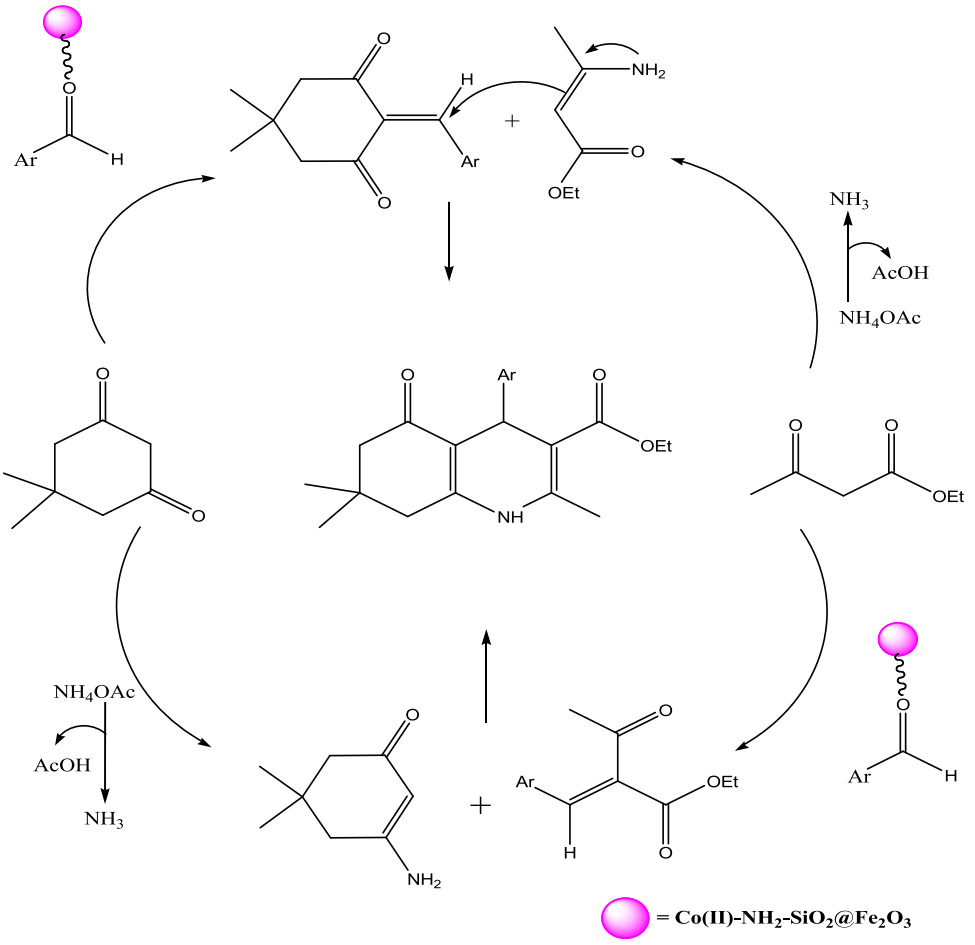

aldehydes with active methylene groups to produce α, β-unsaturated carbonyl compounds and in the Michael addition of intermediates to produce polyhdroquinolines.

3.2. Catalytic Testing in the One-Pot Synthesis of Quinazoline Derivatives. On the ongoing application of the developed nanocatalyst, we were interested in finding an efficient method for the synthesis of quinazoline derivatives. For this, *p*-chlorobenzaldehyde, dimedone, and urea were selected as model substrates. The reaction was optimized under different conditions in terms of solvent, temperature, and amount of catalyst. All of the results are summarized in Table 5. First, we checked the efficiency of Co(II)-NH_2-SiO_2@ Fe_2O_3 as a heterogeneous nanocatalyst by taking different amounts of it. Favorable results were attained with 50 mg of catalyst (Table 6, entry 8). On examining the effect of different solvents, the best yield of product was achieved with an ethanol:water (1:1) mixture (Table 6, entries 5−9). It was found that the optimized reaction temperature of 60 °C was the best and higher temperatures up to 100 °C did not improve the yield of the product (Table 6, entries 5−11).

We tested a series of different aldehydes in the synthesis of quinazoline derivatives using the above-optimized reaction conditions. As shown in Table 5, aldehydes substituted with an electron-withdrawing group led to products with a higher yield in a comparatively short reaction time. Moreover, heterocyclic aldehydes were also efficiently converted into corresponding products with good yields. We also attempted to carry out a reaction with 20 mg of Co(II)- SiO_2@Fe_2O_3 in an ethanol/water (1:1) mixture at room temperature (r.t.), but we did not achieve satisfactory results (Table 6, entry 3). However, the reaction did not start at all in the absence of a catalyst.

A plausible mechanism for the synthesis of quinazolines is shown in Scheme 3. It is presumed that the role of Co(II) was to increase the electrophilicity of the carbonyl group of dimedone and aldehyde. Thus, the first step was the Knoevenagel condensation between the aldehyde and dimedone to generate the adduct, which acted as a Michael acceptor (A). Then, urea attacked (A) to produce a series of intermediates, which finally, upon intramolecular cyclization, produced the final product.[56]

3.2.1. Recyclability. Recyclability and deactivation are of utmost importance to evaluate the efficiency of the heterogeneous catalyst. The recyclability of Co(II)-NH_2-SiO_2@Fe_2O_3 was checked in the case of Table 2, entry 1, for the synthesis of polyhydroquinoline and Table 5, entry 2, for the formation of quinazoline derivatives under optimized conditions and found to be active for five consecutive runs. After the completion of the reaction, the catalyst was recovered by filtration, followed by washing with water, ethanol, and ethyl acetate. The recycled catalyst was characterized by P-XRD and HR-TEM to understand the reasons behind the decline of yield (%), as shown in Figures 3c and 9c. HR-TEM images of the recycled catalyst indicated the disruption of the original layered structure of the catalyst, leading to a decrease

https://doi.org/10.1021/acsomega.2c04512
ACS Omega 2022, 7, 47619−47633

Table 5. Effect of Different Aldehydes in the One-Pot Synthesis of Quinazoline Derivatives Catalyzed by Co(II)-NH_2-SiO_2@Fe_2O_3[a]

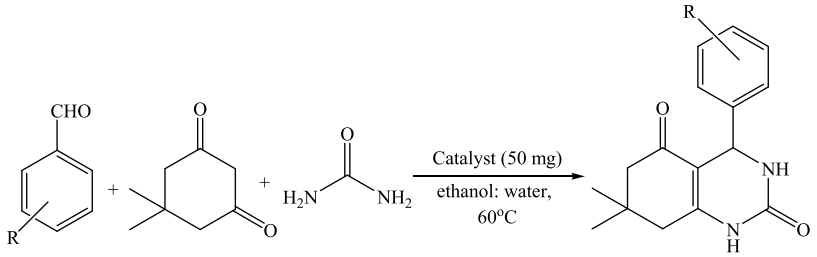

entry	R	time (min)	yield (%)[b]	product
1	H	8	95	5a
2	4-Cl	8	94	5b
3	4-NO_2	9	94	5c
4	4-Br	8	94	5d
5	4-CH_3	12	93	5e
6	2-NO_2	13	92	5f
7	4-OCH_3	12	93	5g
8	2,3-Cl	8	94	5h
9	2,6-F	9	94	5i
10	4-OH	12	92	5j
11	2-OH	15	92	5k
12	2-furyl	16	90	5l
13	2-thienyl	18	89	5m
14	3-indole	16	90	5n

[a]Optimized reaction conditions: aldehyde (1 mmol), dimedone (1 mmol), urea (1 mmol), catalyst (0.05 g), ethanol:H_2O (1:1), 60 °C. [b]Isolated yields.

Table 6. Optimization of Reaction Conditions for the Synthesis of Quinazolines[a]

entry	catalyst (mg)	temp. (°C)	solvents	time (min)	yield (%)[b]
1		r.t.	ethanol	60	
2	Fe_2O_3	60	ethanol: H_2O (1:1)	60	
3	Co(II)-SiO_2@ Fe_2O_3(20)	r.t.	ethanol: H_2O (1:1)	60	65
4	NH_2-SiO_2@ Fe_2O_3	80	ethanol: H_2O (1:1)	60	
5	Co(II)-NH_2-SiO_2@Fe_2O_3(20)	80	ethanol: H_2O (1:1)	25	75
6	Co(II)-NH_2-SiO_2@Fe_2O_3(40)	60	ethanol: H_2O (1:1)	18	82
7	Co(II)-NH_2-SiO_2@Fe_2O_3(50)	80	ethanol: H_2O (1:1)	8	92
8	**Co(II)-NH_2-SiO_2@Fe_2O_3(50)**	**60**	**ethanol: H_2O (1:1)**	**8**	**92**
9	Co(II)-NH_2-SiO_2@Fe_2O_3(50)	100	ethanol: H_2O (1:1)	8	92
10	Co(II)-NH_2-SiO_2@Fe_2O_3(50)	60	CH_3CN	30	59
11	Co(II)-NH_2-SiO_2@Fe_2O_3(50)	60	H_2O	15	90

[a]Optimized reaction conditions: 4-chlorobenzaldehyde (1 mmol), dimedone (1 mmol), urea (1 mmol), catalyst (0.05 g), ethanol:H_2O (1:1), 60 °C. [b]Isolated yields.

in catalytic activity. The polycrystalline nature of the catalyst was retained, as depicted in Figure 9d. However, agglomeration was also observed, which was another reason for the decline after the fifth run of recyclability.[57,58]

4. CONCLUSIONS

In the present work, an efficient and inexpensive nanocatalyst, *i.e.*, Co(II)-NH_2-SiO_2@Fe_2O_3 nanocatalyst, was successfully synthesized, choosing waste toner powder for the Fe_2O_3 core, thus making it an overall environment-friendly system. The various characterization techniques displayed the successful coating and functionalization around Fe_2O_3 with Co(II) loading on the surface. HR-TEM revealed that the core consisted of clusters of polycrystalline Fe_2O_3 nanoparticles having a spherical geometry. Co(II)-NH_2-SiO_2@Fe_2O_3 was utilized in the synthesis of commercially bioactive heterocycles such as polyhydroquinoline and quinazoline derivatives with a wide range of electronically diverse substrates. Subsequently, high yields were obtained in mild reaction conditions. Moreover, the catalyst showed excellent reusability up to five consecutive runs of recyclability with a negligible loss in the yield of products. The reused or recycled catalyst after the fifth run was characterized by HR-TEM and P-XRD spectroscopic techniques to know the structural description. HR-TEM images of the recovered catalyst confirmed the disordering of the catalytic structure after the fifth run.

■ ASSOCIATED CONTENT

Supporting Information

The Supporting Information is available free of charge at https://pubs.acs.org/doi/10.1021/acsomega.2c04512.

https://doi.org/10.1021/acsomega.2c04512
ACS Omega 2022, 7, 47619−47633

Scheme 3. Reasonable Mechanism for the Synthesis of Quinazolines in the Presence of the Co(II)-NH_2-SiO_2@Fe_2O_3 Catalyst

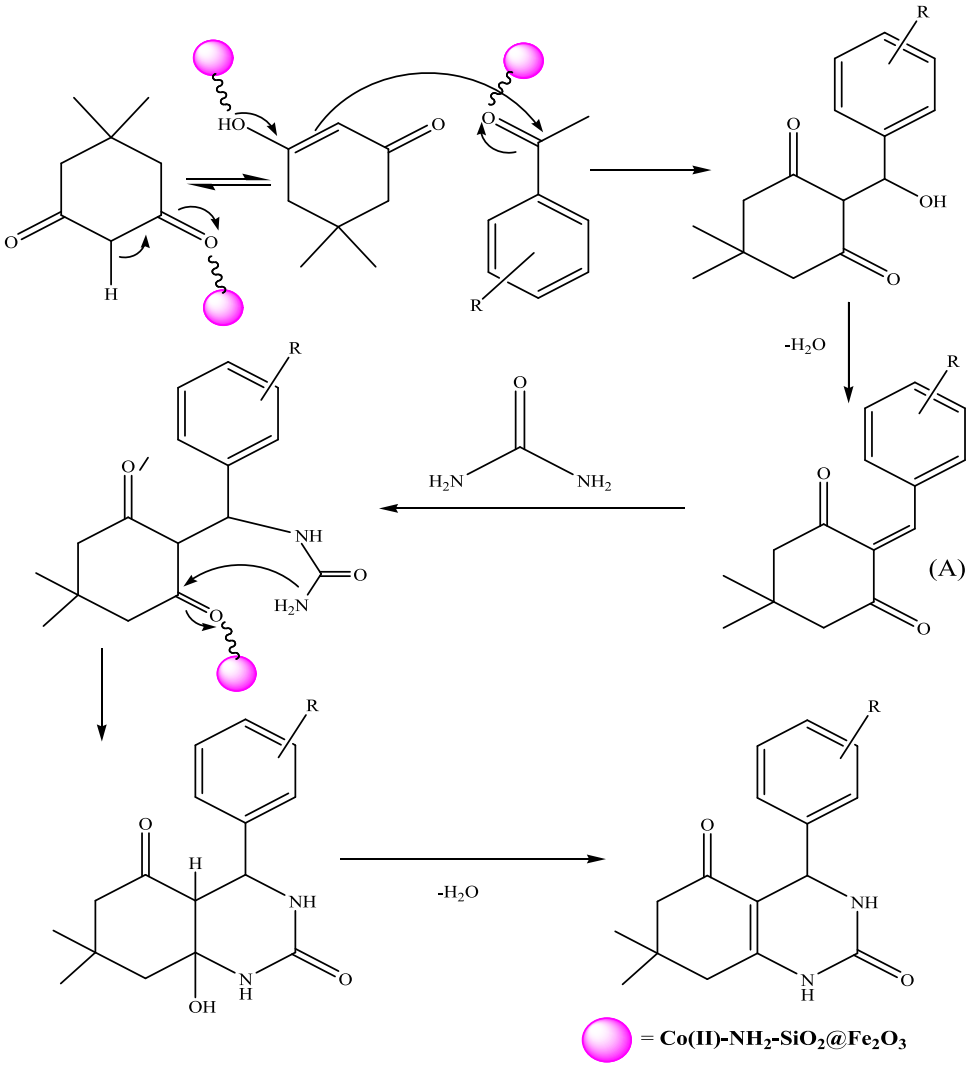

Spectral details and ^1H and ^{13}C NMR spectra of some of the synthesized compounds (PDF)

AUTHOR INFORMATION

Corresponding Author

Monika Gupta − *PG Department of Chemistry, University of Jammu, Jammu 180006, India;* orcid.org/0000-0001-5265-0388; Email: monika.gupta77@rediffmail.com

Authors

Mobina Kouser − *PG Department of Chemistry, University of Jammu, Jammu 180006, India;* orcid.org/0000-0002-3829-5516

Bushra Chowhan − *PG Department of Chemistry, University of Jammu, Jammu 180006, India;* orcid.org/0000-0003-2101-1529

Neha Sharma − *PG Department of Chemistry, University of Jammu, Jammu 180006, India;* orcid.org/0000-0003-2468-3419

Complete contact information is available at: https://pubs.acs.org/10.1021/acsomega.2c04512

Author Contributions

M. K. contributed in the conceptualization, data curation, formal analysis, funding acquisition, investigation, methodology, and software. B. C. contributed in data curation, formal analysis, investigation, and software. N. S. contributed in data curation, formal analysis, investigation, software, and visualization. M. G. contributed in conceptualization, data curation, formal analysis, investigation, methodology, project administration, software, supervision, validation, and visualization.

Notes

The authors declare no competing financial interest.

ACKNOWLEDGMENTS

The authors gratefully acknowledge IIT Roorkee for XPS, VSM, and P-XRD and SAIF, IIT Bombay, for FEG-SEM, HR-TEM, and ICP-AES. The authors also acknowledge DST PURSE, UGC-SAP, and RUSA 2.0 for NMR, FTIR, TGA, and BET, respectively. The authors are grateful to HRDG-CSIR and UGC New Delhi, India, for financial support to authors Mobina Kouser (SRF, File. No.: 09/100(0248)/2020-EMR-1), Bushra Chowhan (SRF, File. No.: 09/100(0199)/2017-EMR-1), and Neha Sharma (SRF, Reference no.: 19/06/2016(i) Eu-V).

https://doi.org/10.1021/acsomega.2c04512
ACS Omega 2022, 7, 47619−47633

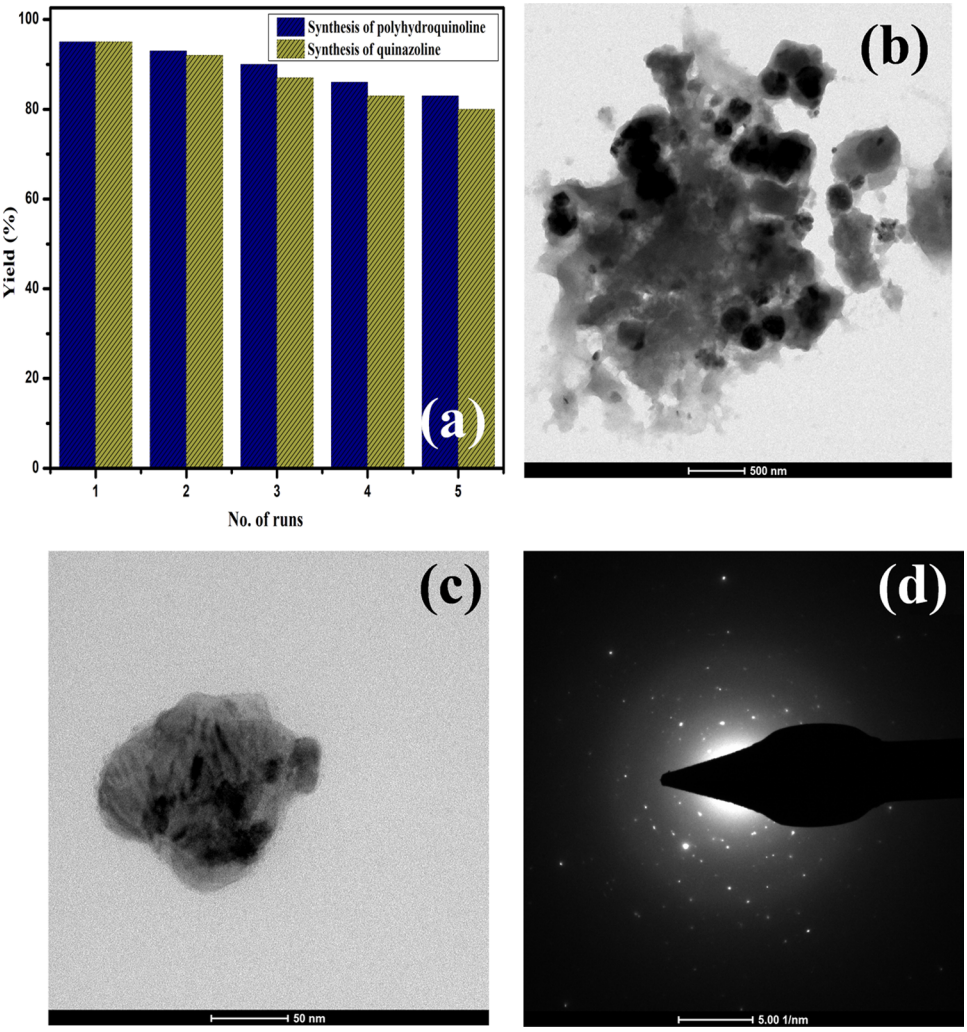

Figure 9. Recyclability graph for Co(II)-NH_2-SiO_2@Fe_2O_3 taking p-chlorobenzaldehyde as a test substrate for both reactions under optimized conditions (a). HR-TEM images of the recycled catalyst showing disruption of the catalytic layered structure (b, c). SAED pattern of the recycled catalyst (d).

REFERENCES

(1) Olveira, S.; Forster, S. P.; Seeger, S. Nanocatalysis: academic discipline and industrial realities. *J. Nanotechnol.* **2014**, *2014*, No. 324089.

(2) Babu, S. G.; Karvembu, R. Copper based nanoparticles-catalyzed organic transformations. *Catal. Surv. Asia* **2013**, *17*, 156−176.

(3) Kaipannan, S.; Govindarajan, K.; Sundaramoorthy, S.; Marappan, S. Waste toner-derived carbon/Fe_3O_4 nanocomposite for high-performance supercapacitor. *ACS Omega* **2019**, *4*, 15798−15805.

(4) Ruan, J.; Li, J.; Xu, Z. An environmental friendly recovery production line of waste toner cartridges. *J. Hazard. Mater.* **2011**, *185*, 696−702.

(5) Ruan, J.; Dong, L.; Huang, J.; Huang, Z.; Huang, K.; Dong, H.; Zhang, T.; Qiu, R. Vacuum-Gasification-Condensation of Waste Toner to Produce Industrial Chemicals and Nanomaterials. *ACS Sustainable Chem. Eng.* **2017**, *5*, 4923−4929.

(6) Gaikwad, V.; Kumar, U.; Pahlevani, F.; Piadasa, A.; Sahajwalla, V. Thermal Transformation of Waste Toner Powder into a Value Added Ferrous Resource. *ACS Sustainable Chem. Eng.* **2017**, *5*, 11543−11550.

(7) Li, Y.; Mao, J.; Xie, H.; Li, J. Heat-Treatment Recycling of Waste Toner and Its Applications in Lithium Ion Batteries. *J. Mater. Cycles Waste Manage.* **2018**, *20*, 361−368.

(8) Yordanova, D.; Angelova, S.; Dombalov, I. Utilisation Options for Waste Toner Powder. *J. Environ. Sci.* **2014**, *3*, 140−144.

(9) Tian, Z.; Sun, L.; Tian, H.; Cao, K.; Bai, S.; Li, J.; Zhu, Q. 3D Graphene Oxide Hydrogel Derived from Waste Toner as Adsorbent. *J. Nanosci. Nanotechnol.* **2021**, *21*, 5275−5281.

(10) Balgude, S.; Godase, S.; Shinde, A.; Harak, C. Succinate assisted synthesis of magnetically separable Fe_2O_3/g-C_3N_4 nano-heterostructure: A stable catalyst for environmental remediation. *Curr. Opin. Green Sustainable Chem.* **2021**, *4*, No. 100210.

(11) Saini, D.; Aggarwal, R.; Anand, S. R.; Satrawala, N.; Joshi, R. K.; Sonkar, S. K. Sustainable feasibility of waste printer ink to magnetically separable iron oxide−doped nanocarbons for styrene oxidation. *Mater. Today Chem.* **2020**, *16*, No. 100256.

(12) Zasonska, B. A.; Boiko, N.; Klyuchivska, O.; Trchová, M.; Petrovský, E.; Stoika, R.; Horák, D. Silica-coated γ-Fe_2O_3 nanoparticles: Preparation and engulfment by mammalian macrophages. *J. Nanopharmaceutics Drug Delivery* **2013**, *1*, 182−192.

(13) Pereira, C.; Pereira, A. M.; Quaresma, P.; Tavares, P. B.; Pereira, E.; Araújo, J. P.; Freire, C. Superparamagnetic γ-Fe_2O_3@ SiO_2 nanoparticles: a novel support for the immobilization of [VO(acac)$_2$]. *Dalton Trans.* **2010**, *39*, 2842−2854.

(14) Burleigh, M. C.; Markowitz, M. A.; Spector, M. S.; Gaber, B. P. Direct synthesis of periodic mesoporous organosilicas: functional incorporation by co-condensation with organosilanes. *J. Phys. Chem. B* **2001**, *105*, 9935−9942.

(15) Wei, Q.; Nie, Z. R.; Hao, Y. L.; Liu, L.; Chen, Z. X.; Zou, J. X. Effect of synthesis conditions on the mesoscopical order of

https://doi.org/10.1021/acsomega.2c04512
ACS Omega 2022, 7, 47619−47633

mesoporous silica SBA-15 functionalized by amino groups. *J. Sol-Gel Sci. Technol.* **2006**, *39*, 103−109.
(16) Burkett, S. L.; Sims, S. D.; Mann, S. Synthesis of hybrid inorganic−organic mesoporous silica by co-condensation of siloxane and organosiloxane precursors. *Chem. Commun.* **1996**, *11*, 1367−1368.
(17) Mercier, L.; Pinnavaia, T. J. Direct synthesis of hybrid organic-inorganic nanoporous silica by a neutral amine assembly route: structure-function control by stoichiometric incorporation oforgano-siloxane molecules. *Chem. Mater.* **2000**, *12*, 188−196.
(18) Guo, C. S.; Weng, C. M.; Hong, F. E. Preparation of Cobalt-Containing Ligands with NHC-and/or P-Coordinating Sites and their application in Heck Reactions: The Formation of an Unexpected Cobalt-Containing Zwitterionic Complex. *Eur. J. Inorg. Chem.* **2010**, *2010*, 3220−3228.
(19) Hammann, J. M.; Haas, D.; Knochel, P. Cobalt-catalyzed negishi cross-coupling reactions of (hetero) arylzinc reagents with primary and secondary alkyl bromides and iodides. *Angew. Chem., Int. Ed.* **2015**, *54*, 4478−4481.
(20) Biggs-Houck, J. E.; Younai, A.; Shaw, J. T. Recent advances in multicomponent reactions for diversity-oriented synthesis. *Curr. Opin. Chem. Biol.* **2010**, *14*, 371−382.
(21) Touré, B. B.; Hall, D. G. Natural product synthesis using multicomponent reaction strategies. *Chem. Rev.* **2009**, *109*, 4439−4486.
(22) Treesa, G. S. S.; Neetha, M.; Saranya, S.; Anilkumar, G. Cobalt-Catalyzed Multi-Component Reactions: Recent Advances and Perspectives in Organic Synthesis. *ChemistrySelect* **2020**, *5*, 7400−7416.
(23) Ghorbani-Choghamarani, A.; Azadi, G. Synthesis, characterization, and application of Fe_3O_4-SA-PPCA as a novel nanomagnetic reusable catalyst for the efficient synthesis of 2, 3-dihydroquinazolin-4 (1*H*)-ones and polyhydroquinolines. *RSC Adv.* **2015**, *5*, 9752−9758.
(24) Rostami, A.; Tahmasbi, B.; Gholami, H.; Taymorian, H. Supported *N*-propylsulfamic acid on magnetic nanoparticles used as recoverable and recyclable catalyst for the synthesis of 2, 3-dihydroquinazolin-4 (1*H*)-ones in water. *Chin. Chem. Lett.* **2013**, *24*, 211−214.
(25) Vahdat, S. M.; Chekin, F.; Hatami, M.; Khavarpour, M.; Baghery, S.; Roshan-Kouhi, Z. Synthesis of polyhydroquinoline derivatives *via* a four-component Hantzsch condensation catalyzed by tin dioxide nanoparticles. *Chin. J. Catal.* **2013**, *34*, 758−763.
(26) Nasr-Esfahani, M.; Hoseini, S. J.; Montazerozohori, M.; Mehrabi, R.; Nasrabadi, H. Magnetic Fe_3O_4 nanoparticles: efficient and recoverable nanocatalyst for the synthesis of polyhydroquinolines and Hantzsch 1, 4-dihydropyridines under solvent-free conditions. *J. Mol. Catal. A: Chem.* **2014**, *382*, 99−105.
(27) Abdolmohammadi, S.; Karimpour, S. Rapid and mild synthesis of quinazolinones and chromeno[*d*]pyrimidinones using nanocrystalline copper (I) iodide under solvent-free conditions. *Chin. Chem. Lett.* **2016**, *27*, 114−118.
(28) Ghosh, A.; Shee, S.; Biju, A. T. A benzannulation strategy for rapid access to Quinazoline-2, 4-diones *via* oxidative *N*-heterocyclic carbene catalysis. *Org. Lett.* **2022**, *24*, 2772−2777.
(29) Mohammadkhani, L.; Heravi, M. M. Microwave-assisted synthesis of quinazolines and quinazolinones: an overview. *Front. Chem.* **2020**, *8*, No. 580086.
(30) Portela-Cubillo, F.; Scott, J. S.; Walton, J. C. Microwave-promoted syntheses of quinazolines and dihydroquinazolines from 2-aminoarylalkanone O-phenyl oximes. *J. Org. Chem.* **2009**, *74*, 4934−4942.
(31) Darvatkar, N. B.; Bhilare, S. V.; Deorukhkar, A. R.; Raut, D. G.; Salunkhe, M. M. [bmim] HSO_4: an efficient and reusable catalyst for one-pot three-component synthesis of 2, 3-dihydro-4 (1*H*)-quinazolinones. *Green Chem. Lett. Rev.* **2010**, *3*, 301−306.
(32) Zhang, Y.; Xu, Q.; Zhang, S.; Liu, J.; Zhou, J.; Xu, H.; Xiao, H.; Li, J. Preparation of thiol-modified Fe_3O_4@SiO_2 nanoparticles and their application for gold recovery from dilute solution. *Sep. Purif. Technol.* **2013**, *116*, 391−397.
(33) Sharma, N.; Chowhan, B.; Gupta, M.; Kouser, M. $NiFe_2O_4$@B, N, F-tridoped CeO_2 (NFTDNC): a mesoporous nanocatalyst in the synthesis of pyrazolopyranopyrimidine and 1 H-pyrazolo [1, 2-b] phthalazine-5, 10-dione derivatives and as an adsorbent. *Dalton Trans.* **2022**, *51*, 13795−13807.
(34) Zhang, L. Y.; Zhang, W.; Zhou, Z.; Li, C. M. γ-Fe_2O_3 nanocrystals-anchored macro/meso-porous graphene as a highly efficient adsorbent toward removal of methylene blue. *J. Colloid Interface Sci.* **2016**, *476*, 200−205.
(35) Zhang, F.; Li, X.; Zhao, Q.; Zhang, Q.; Tadé, M.; Liu, S. Fabrication of α-Fe_2O_3/In_2O_3 composite hollow microspheres: A novel hybrid photocatalyst for toluene degradation under visible light. *J. Colloid Interface Sci.* **2015**, *457*, 18−26.
(36) Babar, S.; Gavade, N.; Shinde, H.; Gore, A.; Mahajan, P.; Lee, K. H.; Bhuse, V.; Garadkar, K. An innovative transformation of waste toner powder into magnetic g-C_3N_4-Fe_2O_3 photocatalyst: sustainable e-waste management. *J. Environ. Chem. Eng.* **2019**, *7*, No. 103041.
(37) Lin, Y.; Sun, F. Q.; Yuan, X. Y.; Geng, B. Y.; Zhang, L. D. Sol−gel electrophoretic deposition and optical properties of Fe_2O_3 nanowire arrays. *Appl. Phys. A: Mater. Sci. Process.* **2004**, *78*, 1197−1199.
(38) Darezereshki, E.; Ranjbar, M.; Bakhtiari, F. One-step synthesis of maghemite (γ-Fe_2O_3) nano-particles by wet chemical method. *J. Alloys Compd.* **2010**, *502*, 257−260.
(39) Kite, S. V.; Kadam, A. N.; Sathe, D. J.; Patil, S.; Mali, S. S.; Hong, C. K.; Lee, S. W.; Garadkar, K. M. Nanostructured TiO_2 sensitized with MoS_2 nanoflowers for enhanced photodegradation efficiency toward methyl orange. *ACS Omega* **2021**, *6*, 17071−17085.
(40) Huang, C.; Li, H.; Yang, J.; Wang, C.; Hu, F.; Wang, X.; Lu, Z. H.; Feng, G.; Zhang, R. Ce0. 6Zr0. 3Y0. $1O_2$ solid solutions-supported NiCo bimetal nanocatalysts for NH_3 decomposition. *Appl. Surf. Sci.* **2019**, *478*, 708−716.
(41) Borod'Ko, Y. G.; Vetchinkin, S. I.; Zimont, S. L.; Ivleva, I. N.; Shul'Ga, Y. M. Nature of satellites in X-ray photoelectron spectra XPS of paramagnetic cobalt (II) compounds. *Chem. Phys. Lett.* **1976**, *42*, 264−267.
(42) Bazylewski, P.; Boukhvalov, D. W.; Kukharenko, A. I.; Kurmaev, E. Z.; Hunt, A.; Moewes, A.; Lee, Y. H.; Cholakh, S. O.; Chang, G. S. The characterization of Co-nanoparticles supported on graphene. *RSC Adv.* **2015**, *5*, 75600−75606.
(43) Sarkar, M.; Banerjee, A.; Pramanick, P. P.; Sarkar, A. R. Use of laterite for the removal of fluoride from contaminated drinking water. *J. Colloid Interface Sci.* **2006**, *302*, 432−441.
(44) Palimi, M. J.; Rostami, M.; Mahdavian, M.; Ramezanzadeh, B. Surface modification of Fe_2O_3 nanoparticles with 3-aminopropyl-trimethoxysilane (APTMS): an attempt to investigate surface treatment on surface chemistry and mechanical properties of polyurethane/Fe_2O_3 nanocomposites. *Appl. Surf. Sci.* **2014**, *320*, 60−72.
(45) Mangesh, K.; Dapurkar, S.; Garadkar, K.; Gole, A. Magnetite−silica−gold nanocomposite: one-pot single-step synthesis and its application for solvent-free oxidation of benzyl alcohol. *J. Phys. Chem. C* **2015**, *119*, 14214−14223.
(46) Trino, L. D.; Dias, L. F.; Albano, L. G.; Bronze-Uhle, E. S.; Rangel, E. C.; Graeff, C. F.; Lisboa-Filho, P. N. Zinc oxide surface functionalization and related effects on corrosion resistance of titanium implants. *Ceram. Int.* **2018**, *44*, 4000−4008.
(47) Serre, C.; Calvo-Barrio, L.; Pérez-Rodríguez, A.; Romano-Rodríguez, A.; Morante, J. R.; Pacaud, Y.; Kögler, R.; Heera, V.; Skorupa, W. Ion-beam synthesis of amorphous SiC films: structural analysis and recrystallization. *J. Appl. Phys.* **1996**, *79*, 6907−6913.
(48) Yordanova, D.; Angelova, S.; Dombalov, I. Utilisation options for waste toner powder. *J. Environ. Sci* **2014**, *3*, 140−144.
(49) Duraes, L.; Costa, B. F. O.; Vasques, J.; Campos, J. and Portugal, A. Phase investigation of as-prepared iron oxide/hydroxide produced by sol−gel synthesis. *Mater Lett.* **2005**, *59*, 859−863.
(50) Glisenti, A. Interaction of formic acid with Fe_2O_3 powders under different atmospheres: an XPS and FTIR study. *J. Chem. Soc., Faraday Trans.* **1998**, *94*, 3671−3676.

https://doi.org/10.1021/acsomega.2c04512
ACS Omega 2022, 7, 47619−47633

(51) Feng, G.; Huo, C. F.; Li, Y. W.; Wang, J.; Jiao, H. Structures and energies of iron promoted γ-Al_2O_3 surface: A computational study. *Chem. Phys. Lett.* **2011**, *510*, 224−227.
(52) Joshi, D. P.; Pant, G.; Arora, N.; Nainwal, S. Effect of solvents on morphology, magnetic and dielectric properties of (α-Fe_2O_3@ SiO_2) core-shell nanoparticles. *Heliyon* **2017**, *3*, No. e00253.
(53) Ziyadi, H.; Heydari, A.; Rezayat, S. M. Preparation and characterization of magnetic α-Fe_2O_3 nanofibers coated with uniform layers of silica. *Ceram. Int.* **2014**, *40*, 5913−5919.
(54) Li, L.; Gan, Y. M.; Lu, Z. H.; Qing, S.; Gao, Z.; Zhang, R.; Feng, G. The effects of Fe, Co and Ni doping in $CuAl_2O_4$ spinel surface and bulk: A DFT study. *Appl. Surf. Sci.* **2020**, *521*, No. 146478.
(55) Hajjami, M.; Tahmasbi, B. Synthesis and characterization of glucosulfonic acid supported on Fe_3O_4 nanoparticles as a novel and magnetically recoverable nanocatalyst and its application in the synthesis of polyhydroquinoline and 2, 3-dihydroquinazolin-4 (1 H)-one derivatives. *RSC Adv.* **2015**, *5*, 59194−59203.
(56) Ghasemzadeh, M. A.; Ghaffarian, F. Preparation of core/shell/shell CoFe2O4/OCMC/Cu (BDC) nanostructure as a magnetically heterogeneous catalyst for the synthesis of substituted xanthenes, quinazolines and acridines under ultrasonic irradiation. *Appl. Organomet. Chem.* **2020**, *34*, No. e5580.
(57) Chowhan, B.; Gupta, M.; Sharma, N. Fabrication and characterization of adenine-grafted carbon-modified amorphous ZnO with enhanced catalytic activity. *Appl. Organomet. Chem.* **2020**, *34*, No. e6013.
(58) Sharma, N.; Gupta, M.; Chowhan, B.; Frontera, A. Magnetically separable nanocatalyst (IL@$CuFe_2O_4$-L-Tyr-TiO_2/TiTCIL): Preparation, characterization and its applications in 1, 2, 3-triazole synthesis and in photodegradation of MB. *J. Mol. Struct.* **2021**, *1224*, No. 129029.

https://doi.org/10.1021/acsomega.2c04512
ACS Omega 2022, 7, 47619−47633